

Fermi points and topological quantum phase transitions in a model of superconducting wires

T.O. Puel^{1,*}, P.D. Sacramento^{1,2}, and M. A. Continentino¹

¹*Centro Brasileiro de Pesquisas Físicas, Rua Dr. Xavier Sigaud, 150, Urca 22290-180, Rio de Janeiro, RJ, Brazil and*

²*CeFEMA, Instituto Superior Técnico, Universidade de Lisboa, Av. Rovisco Pais, 1049-001 Lisboa, Portugal*

(Dated: July 30, 2018)

The importance of models with an exact solution for the study of materials with non-trivial topological properties has been extensively demonstrated. Among these, the Kitaev model of a one-dimensional p-wave superconductor plays a guiding role in the search for Majorana modes in condensed matter systems. Also, the sp chain, with an anti-symmetric mixing among the s and p bands provides a paradigmatic example of a topological insulator with well understood properties. There is an intimate relation between these two models and in particular their topological quantum phase transitions share the same universality class. Here we consider a two-band sp model of spinless fermions with an attractive (inter-band) interaction. Both the interaction and hybridization between the s and p fermions are anti-symmetric. The zero temperature phase diagram of the model presents a variety of phases including a Weyl superconductor, topological insulator and trivial phases. The quantum phase transitions between these phases can be either continuous or discontinuous. We show that the transition from the topological superconducting phase to the trivial one has critical exponents different from those of an equivalent transition in Kitaev's model.

I. INTRODUCTION

Since the first strong experimental evidence of Majorana fermions [1] in a hybrid superconductor-semiconductor one dimensional system, the search for exotic states supporting Majorana fermions has attracted increasing interest in condensed matter physics. Recent observations have reinforced the existence of Majorana, specially the one made in ferromagnetic atomic chains on a superconductor (SC) [2]. Anomalous behaviour on this experimental evidence [3] indicates that the appearance of Majorana may have yet unknown sources. Also some technical difficulties such as highly localized states compared to the material parameters [4] or high temperatures that prevent to have access inside the gap [5] have left the existence of Majorana inconclusive. The running for the experimental discovery of Majorana is well described in [6].

It is well known that the Kitaev model [7–9] – anti-symmetric pairs of spinless fermions in 1D – exhibits a non-trivial topological phase with Majorana modes at the ends of a p -wave superconducting chain. The excitations at the ends of the chain depend on the quantum state of the system, which in turn is determined by the ratio $\mu/2t$, between the chemical potential μ and the hopping t . If $|\mu|/2t < 1$ the chain is superconducting with non-trivial topological properties. This *weak pairing* phase presents Majorana fermions at its ends. Otherwise, if $|\mu|/2t > 1$ the chain is in a *strong coupling* superconducting phase with trivial topological properties and has no end states [9].

The importance of the mixing of sp bands for topological insulators has already been pointed out in differ-

ent contexts, including that of the spin quantum Hall effect [10] and a cold atom version of the sp -chain, the sp -ladder[11]. The sp mixing is in a special class that mixes orbitals with angular momenta that differ by an odd number. This implies the anti-symmetric property $V(-\mathbf{r}) = -V(\mathbf{r})$ or in momentum space $V(-\mathbf{k}) = -V(\mathbf{k})$ [12].

In addition, it was recently shown [13–15] an intimate relation between a two band insulator with anti-symmetric hybridization and the Kitaev model, as regards to the topological properties and their end states. By tuning the parameters of the 1D sp chain, the system can be driven, through a topological quantum phase transition, from a trivial to a topological insulator. As a result they found two Majorana zero modes at the ends of an insulating chain. In the search for Majorana modes, Kitaev's model is a most clear example of the importance of exactly soluble models as guides in this difficult path.

Here we consider a different model of a p -wave superconducting chain that also can be solved exactly. This study will throw further light on the role of topology and different type of interactions and symmetry breaking terms as conditions for the existence of Majorana in superconducting wires. We consider a two-band model of spinless fermions in a chain with inter-band attractive interactions and an anti-symmetric hybridization. The model is exactly soluble and we obtain its zero temperature phase diagram. For a fixed small value of the mixing, as the ratio $\mu/2t$ of the model increases, such that $|\mu|/2t > 1$, there is a topological quantum phase transition from a gapless (topologically non-trivial) to a gapped (trivial) superconducting phase. The phase diagram resembles that of Kitaev's model, however the nature of the topological phases, as well as, the topological transition are distinct. In our model the non-trivial superconducting phase has gapless Fermi points. These

* tharnier@me.com

gapless points have the characteristic of Weyl fermions in 3D systems [16–18], as they have a non-degenerated linear dispersion relation and appear or disappear in pairs, only when two Fermi points unite. The conservation of the *topological charge* associated with these Fermi points [19] confers a non-trivial topological character for this phase. Furthermore, we show that the topological quantum phase transition at $(|\mu|/2t)_c = 1$ is in a different universality class of that of Kitaev’s model. Next, fixing the chemical potential, say at $\mu = 0$, and increasing the hybridization the system is driven from the Weyl superconducting phase (WSC) to a topological insulator through a first order quantum phase transition. Topological phase transitions are known to produce anomalies in thermodynamic quantities[20] and we obtain these here, with special emphasis on the behaviour of the compressibility.

In section II we define the model and analyse the superconductivity stability. In section III we show the phase diagram for the superconducting stability. We also discuss the nature of the transitions and show the localization of end states in a finite system. In section IV we calculate topological invariants of different phases, and discuss the topological properties of the model in Majorana basis. Finally, in section V we present some conclusions and highlight the main results.

II. DEFINING THE MODEL

We consider a two-band problem with hybridisation and triplet inter-band superconductivity in 1D, i.e., a chain with two orbitals per site, with angular momenta differing by an odd number, let’s say p and s . The pairing between fermions on different bands (inter-band) is always p -wave kind, in the sense that the pairing of spinless fermions is anti-symmetric. The problem can be viewed as a generalization of Kitaev’s model to two orbitals and only interband pairing. We also have the anti-symmetric hybridisation term that, under some conditions, was shown to be responsible for topological phases[13–15]. The simplest Hamiltonian in the momentum space that describes those types of superconductivity and hybridization can be written as

$$\mathcal{H} = \sum_k \left\{ -\mu \left(c_k^\dagger c_k + p_k^\dagger p_k \right) + 2t \cos(k) \left(p_k^\dagger p_k - c_k^\dagger c_k \right) - i\Delta \sin(k) c_k^\dagger p_{-k}^\dagger + iV \sin(k) c_k^\dagger p_k + \text{h.c.} \right\}, \quad (1)$$

where μ is the chemical potential, Δ is the sp pairing amplitude, and V is the anti-symmetric hybridization amplitude. Note that the hopping amplitude t has different sign in each band, representing particles for the orbital s and holes for the orbital p . We can write the same Hamiltonian using the Bogoliubov-de Gennes (BdG) representation as

$$\mathcal{H} = \sum_k \mathbf{C}_k^\dagger \mathcal{H}_k \mathbf{C}_k, \quad (2)$$

with $\mathbf{C}_k^\dagger = \left(c_k^\dagger p_k^\dagger c_{-k} p_{-k} \right)$ and

$$\mathcal{H}_k = -\mu \Gamma_{z0} - \varepsilon_k \Gamma_{zz} + \Delta_k \Gamma_{yx} - V_k \Gamma_{zy}, \quad (3)$$

where $\Gamma_{ab} = r_a \otimes \tau_b$, $\forall a, b = x, y, z$, and $r_{x,y,z}/\tau_{x,y,z}$ are the Pauli matrices acting on particle-hole/orbitals space, respectively, and $r_0 = \tau_0$ are the 2×2 identity matrix. We have defined $\varepsilon_k = 2t \cos(k)$, $V_k = V \sin(k)$, and $\Delta_k = \Delta \sin(k)$.

A. Energy spectrum

Since a topological phase transition only occurs when a gap closes, looking for gapless points on the energy spectrum may indicate this transition. The model considered here has the following energy dispersion relations,

$$E(k) = \pm \sqrt{Z_1 \pm 2\sqrt{Z_2}}, \quad (4)$$

where $Z_1 = A(k) + B(k)$ and $Z_2 = A(k)B(k)$, with $A(k) = \varepsilon_k^2 + V_k^2$ and $B(k) = \Delta_k^2 + \mu^2$. Looking for gapless points ($E(k) = 0$) the possible solution is $A(k) = B(k)$, i.e.,

$$\begin{aligned} \mu^2 &= \varepsilon_k^2 + V_k^2 - \Delta_k^2 \\ &= \left[(2t)^2 \cos^2(k) + (V^2 - \Delta^2) \sin^2(k) \right]. \end{aligned} \quad (5)$$

We will analyze the equation above more deeply in section III. First we would like to highlight the case with no hybridization, $V = 0$, in which the system is always gapless whenever $|\mu| \leq 2t$. The existence of these gapless modes represents a substantial difference between this and the Kitaev model, see figure 1. We will see in the next section that even in this non-gapped region the system shows superconductivity. On the other side, when $|\mu| > 2t$, the system is fully gapped but superconductivity is still present up to $|\mu| < 4t$.

Deep inside the gapless phase the crossings between bands have a linear dispersion relation (1a) and define Dirac nodes. Furthermore, we note that the bands are non-degenerate and the nodes appear and disappear only when two nodes are combined, as one can see comparing figures 1a and 1b. This is a characteristic of Weyl fermions in 3D or 2D SC[18] and in topological superfluidity[16, 17]. In this sense, the model here presented can be called 1D Weyl SC.

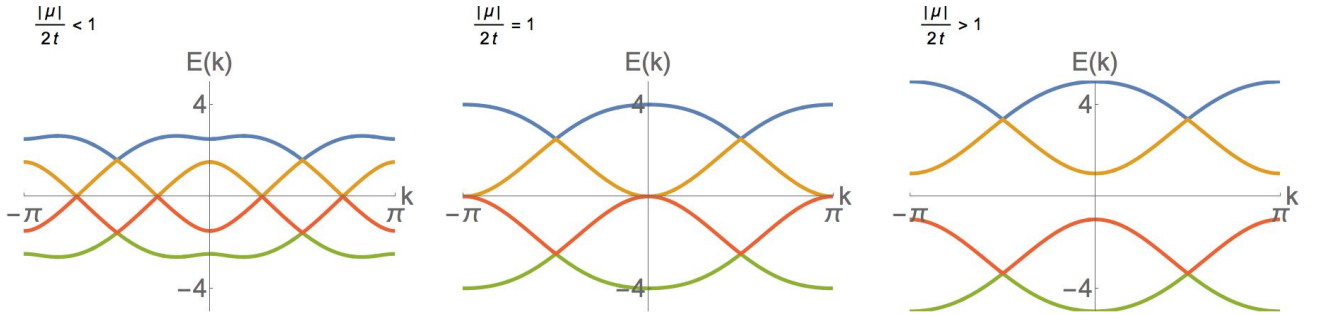


Figure 1. Dispersion relations for a pure sp superconducting system, without hybridization, for $\Delta = 1.5$ and $V = 0$. The system supports gapless excitations when $(|\mu|/2t) < 1$ and is gapped otherwise, specifically, we set $(|\mu|/2t) = 0.25$ (left) and $(|\mu|/2t) = 1.5$ (right). In this work we show that both regions have self-consistent solutions for the superconductivity. The central panel shows the zero modes annihilation; note that it happens in pairs of nodes.

B. Self-consistent equations for the superconductivity and the occupation number

We may calculate the self-consistent inter-band superconducting order parameter, Δ , from the gap equation

$$\Delta = -\frac{4g}{L} \sum_k i \sin(k) \langle p_{-k} c_k \rangle, \quad (6)$$

where, g is the attractive energy between the spinless fermions, L is the length of the chain, and the correlation function $\langle p_{-k} c_k \rangle$ is obtained from the fluctuation-dissipation theorem[21] (a similar calculation was recently done in [12]), such that

$$\langle p_{-k} c_k \rangle = \frac{i}{2\pi} \int f(\omega) [\langle c_k, p_{-k} \rangle^r - \langle c_k, p_{-k} \rangle^a] d\omega; \quad (7)$$

the Green's functions $\langle c_k, p_{-k} \rangle^{r,a}$ (retarded and advanced) are obtained from the Greenian operator [22–24], i.e., $\langle \langle \mathbf{G} \rangle \rangle_k = (\omega \mathbb{I}_{4 \times 4} - \mathcal{H}_k)^{-1}$, and $f(\omega)$ is the Fermi distribution. If we proceed with the calculations, see appendix A, the gap equation at $T=0$ becomes

$$\frac{1}{g} = \frac{1}{L} \sum_k \frac{4 \sin^2(k)}{(\omega_1 + \omega_2)} \delta_k, \quad (8)$$

where

$$\delta_k = \begin{cases} 1 & \text{if } B(k) > A(k), \\ 0 & \text{otherwise.} \end{cases} \quad (9)$$

Also, ω_1 and ω_2 are the eigenvalues of the Hamiltonian, such that,

$$\begin{aligned} \omega_1(k) &\equiv E(k)_+ = \sqrt{Z_1 + 2\sqrt{Z_2}}, \\ \omega_2(k) &\equiv E(k)_- = \sqrt{Z_1 - 2\sqrt{Z_2}}. \end{aligned} \quad (10)$$

We can verify the stability of the superconducting phase calculating the parameters Δ and μ self-consistently from the gap and the occupation number

equation given by,

$$n = n_s + n_p = \frac{1}{L} \sum_k \left[\langle c_k^\dagger c_k \rangle + \langle p_k^\dagger p_k \rangle \right], \quad (11)$$

with n_s and n_p the occupation numbers for the s and p bands, respectively. For the model considered here, the above equation is

$$n = \frac{1}{L} \sum_k \left[\frac{\mu}{(\omega_1 + \omega_2)} \delta_k + \frac{1}{2} \right], \quad (12)$$

where $0 < n < 2$ is the total occupation number per site of the chain.

III. PHASE DIAGRAM

The solution of the coupled self-consistent equations for the gap and the chemical potential is complicated by the constraints of the sums in momentum space (Eq. (9)). In this section we present the phase diagram of our model system obtained directly from a numerical solution of the BdG equations fixing the chemical potential. The Hamiltonian defined in Eq. (3) can be solved using BdG transformations as

$$\begin{aligned} c_k &= \sum_n \left[u_{n,k}^s \gamma_{n,k} + (v_{n,k}^s)^* \gamma_{n,-k}^\dagger \right], \\ p_k &= \sum_n \left[u_{n,k}^p \gamma_{n,k} + (v_{n,k}^p)^* \gamma_{n,-k}^\dagger \right]. \end{aligned} \quad (13)$$

This transformation diagonalizes the Hamiltonian in the form

$$\mathcal{H}_k \begin{pmatrix} u_{n,k}^s \\ u_{n,k}^p \\ v_{n,-k}^s \\ v_{n,-k}^p \end{pmatrix}_n = E_n \begin{pmatrix} u_{n,k}^s \\ u_{n,k}^p \\ v_{n,-k}^s \\ v_{n,-k}^p \end{pmatrix}_n, \quad (14)$$

where E_n are the energy eigenvalues and the wave functions spinor are the eigenstates. The self-consistent solution implies that the pairing can be obtained using

$$\Delta = -\frac{2g}{L} \sum_k i \sin(k) (\langle c_{-k} p_k \rangle + \langle p_{-k} c_k \rangle). \quad (15)$$

At zero temperature, using the representation of the fermionic operators in terms of the wave functions and the Bogoliubov coefficients we may write

$$\Delta = \frac{2g}{L} \sum_k \sum_n i \sin(k) \left[u_{n,k}^s (v_{n,-k}^p)^* + u_{n,k}^p (v_{n,-k}^s)^* \right]. \quad (16)$$

In Fig. 2a we show the numerical results for the order parameter Δ as a function of the chemical potential and hybridization for a fixed value of the attractive interaction $g = 1.7$. All quantities are normalized by the hopping term t . In Fig. 2c we show the gap for excitations for the same range of parameters. The results in these figures allow us to obtain the zero temperature phase diagram of the system shown in Fig. 2b.

In agreement with our previous discussions we find a gapless superconducting phase for $(|\mu|/2t) < 1$ and $V/2t < V_c(\mu)/2t \equiv [(\mu/2t)^2 + (\Delta_0/2t)^2]^{1/2}$ named Weyl SC (*WSC*) in the phase diagram. We note that at the transition ($V = V_c(\mu)$) the gapless points always occur at $k = \pm\pi/2$. The quantity $\Delta_0 = \Delta_0(\mu)$ is the value of the order parameter at $V = 0$ for a given chemical potential value μ .

For $(|\mu|/2t) > 1$ and $V < V_c(\mu)$ the system presents a gapped superconducting phase with trivial topological properties similar to the strong coupling superconducting phase of Kitaev's model. In this phase, named *SC* in the phase diagram, the order parameter vanishes continuously as the chemical potential increases. For a fixed $V < V_c(\mu)$, the range of this phase for increasing $\mu/2t$ depends on the strength of the attractive interaction g .

On the other hand for $(|\mu|/2t) < 1$, but for $V > V_c(\mu)$, there is a gapped non-superconducting phase, that corresponds to a topological insulator (*TI*), as will be discussed below. This phase is characterized by zero energy modes localized at the ends of the chain for $\mu = 0$. There are also localized modes if $\mu \neq 0$ that have finite subgap energy.

Notice that the conditions for the existence of a gap are given by Eq. (5). For instance, in the case of strong hybridization and weak or no superconductivity, such that $1 + (\Delta/2t)^2 < (V/2t)^2$, the system becomes gapless whenever $(\mu/2t) \geq 1$ and $V > V_c(\mu)$. This corresponds to the phase *M* in the phase diagram of figure 2b which is a normal metallic or insulating phase (not shown in the figure) depending on the occupation number.

In order to clarify the understanding of the phases discussed above, in figure 3 we plot the energy spectrum in different regions of the phase diagram of figure 2b. These figures illustrate the cases of appearance of gapped or gapless superconductivity.

A. Nature of the transitions

1. WSC-TI Half-filling

Let us first consider the case of half-filling bands ($n = 1$), where the chemical potential is fixed at $\mu = 0$. The constraint in equation (9) now reads $\Delta_k^2 > (\varepsilon_k^2 + V_k^2)$. Important points in momentum space correspond to those wavevectors where this inequality becomes an equality, i.e.,

$$\tan^2(k_0) = \frac{(2t)^2}{\Delta^2 - V^2}. \quad (17)$$

At these points the system becomes gapless and they characterize the Weyl points. From this result, we can immediately see that there are no gapless nodes when $V > \Delta$. It is easy to see also that with increasing hybridization the Weyl points collapse at $k_0 = \pi/2 \equiv k_F$ for $V = V_c = \Delta$ at a discontinuous quantum phase transition from the WSC to the TI phase where the superconducting order parameter drops to zero. This collapse of superconductivity is associated with the appearance of zero energy modes exactly at the Fermi surface k_F , of the half-filled system. In the superconducting side before the transition, the order parameter (when $\mu = 0$) is given by the gap equation,

$$\frac{1}{g} = \frac{4}{|\Delta|L} \sum_{k=0}^{k_0} \sin(k). \quad (18)$$

where k_0 is the largest momentum value that contributes to the superconductivity. Notice that this equation has no trivial analytic solution since k_0 depends on Δ . At the transition, for $V_c = \Delta$ the momenta $k_0 = \pm\pi/2$ and $\Delta_0 = 4g/2\pi$ before dropping abruptly to zero at the TI phase.

2. WSC-SC

We now investigate the transition from the non-trivial topological superconductor to the trivial one by increasing the chemical potential at fixed hybridization. Let us for simplicity consider the case of $V = 0$. The WSC-SC transition occurs for $(\mu/2t)_c = 1$ as shown in figure 2c. It is associated, as can be easily checked with the collapse of two Weyl points at the center of the Brillouin zone ($k = 0$) and at its extremities ($k = \pm\pi$). Expanding the dispersion relation of the excitations close to $k = 0$ and $(\mu/2t)_c = 1$, we get,

$$\omega_2(k) = 2t \sqrt{\left(1 - \frac{\mu}{2t}\right)^2 + \left(\frac{\Delta}{2t}\right)^2 k^4}. \quad (19)$$

We have omitted the k^2 term, since its coefficient is proportional to $(1 - \mu/2t)$ and vanishes at the quantum topological phase transition at $(\mu/2t)_c = 1$. Then, at

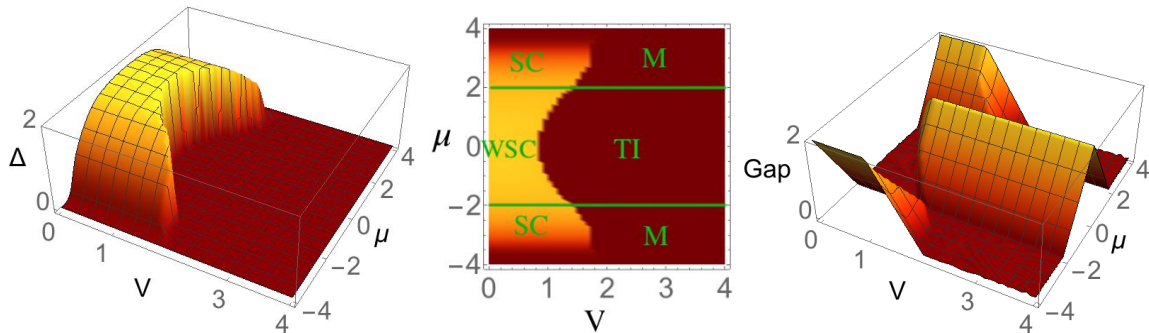


Figure 2. The superconducting amplitude Δ (left panel) and spectrum gap (right panel) for different values of V and μ , with $g = 1.7$. The middle panel shows all the different phases, that are: trivial superconducting gapped phase (SC), metallic (M), gapless Weyl superconductor (WSC) and topological insulator (TI).

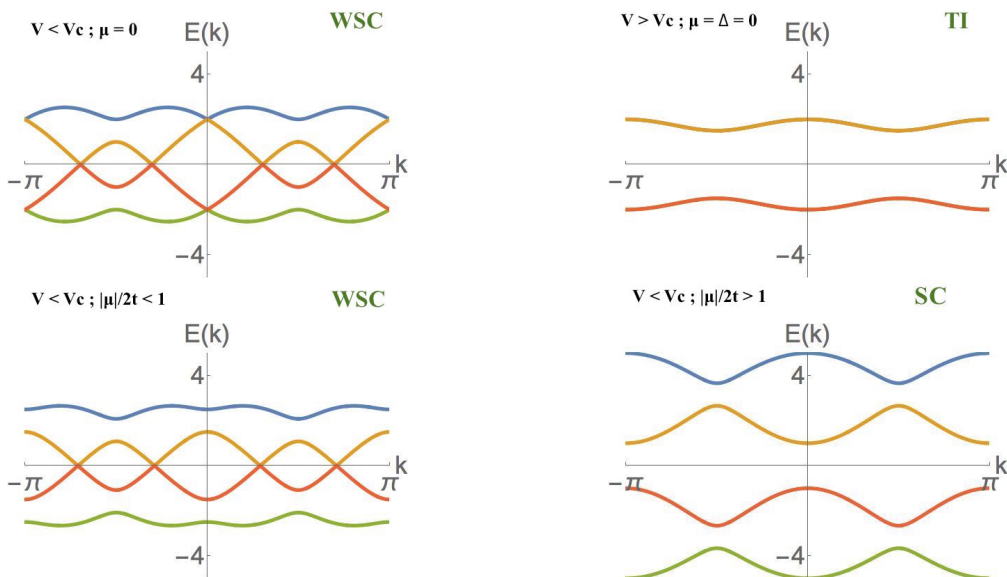


Figure 3. Energy spectrum in momentum space for different points on the phase diagram shown in figure 2. The up left panel shows a system with hybridization and superconductivity when $V < \Delta$, and the chemical potential is fine tuned to zero (specifically, $t = 1$, $\mu = 0$, $V = 0.5$ and $\Delta = 1.5$); the up right panel illustrate the case where there is no self-consistent superconductivity (specifically, $t = 1$, $\mu = \Delta = 0$ and $V = 1.5$). The down panels show the cases where there is superconductivity but the chemical potential is driven out from zero. The left plot has the same conditions that the first case but with $\mu = 0.5$, and it illustrates the case with gapless superconductivity. On the other hand, the right panel was set to same conditions as before but $\mu = 3$ and $\Delta = 1$, and it illustrates the full gapped superconducting region.

the quantum critical point, the spectrum of excitations $\omega_2(k) \propto k^2$, which allows to identify the dynamical exponent $z = 2$ for this transition. On the other hand at $k = 0$, the gap $\omega_2(k = 0) = (\mu/2t)_c - (\mu/2t)$, vanishes linearly at the quantum critical point with a gap exponent $\nu z = 1$. The critical exponents $\nu = 1/2$ and $z = 2$ show that the quantum phase transition from the topological to the trivial superconducting phase in the inter-band model is in a different universality class from that of the Kitaev model. In the latter at the QCP, $(\mu/2t)_c = 1$, the dispersion is linear implying a dynamic exponent $z = 1$. Since the gap vanishes linearly also, we get for the correlation length exponent the

value $\nu = 1$ (see Ref. [14]). These different values of the critical exponents imply distinct behaviour for the compressibility of the two models at the topological quantum phase transition inside the superconducting phase. The compressibility close to this transition is given by, $\chi_c = \partial^2 f / \partial \mu^2 \propto |((\mu/2t)_c - (\mu/2t))|^{-\alpha}$ where f is the free energy density. The exponent α is related to the correlation length and dynamical exponents by the quantum hyperscaling relation [25–27], $2 - \alpha = \nu(d + z)$. It can be easily verified that while for the intra-band Kitaev model $\alpha = 0$, which is generally associated with a logarithmic singularity [28], for the inter-band model $\alpha = 1/2$ implying an even stronger singularity for the compressibility

at the topological transition. Indeed in our model the topological transition is in the universality of the Lifshitz transition [19]. Notice that this is a purely topological quantum phase transition, since both phases are characterised by the same order parameter. In spite of this, they have singularities described by critical exponents which obey the quantum hyperscaling relation [25]. Although the usual Landau approach of expanding the free energy in terms of order parameters that become small close to a continuous phase transition is of no use here, the renormalisation group still provides an adequate description of this critical phenomenon [27].

B. Fermi velocity

We may calculate the Fermi velocity at the Fermi points k_0 expanding the energy spectrum in equation (4) in their vicinity. The spectrum becomes $E(k) = E(k_0) + v_F(k - k_0) + O(k^2)$, where $v_F = v_F(k_0)$ is the Fermi velocity. For the general condition in equation (9) the Fermi points are given by,

$$k_0 = \arcsin \left[\sqrt{\frac{(2t)^2 - \mu^2}{\Delta^2 - V^2 + (2t)^2}} \right], \quad (20)$$

where, of course, the term inside the brackets must be within the range $[0, 1]$. The Fermi velocities were obtained for three different situations and are shown in Fig. 4. The up row shows the variation of k_0 for a system without hybridization ($V = 0$), for a fixed $\Delta = 2$, then for fixed $\Delta = V = 2$, respectively from left to right. The down row shows the Fermi velocities for each case, corresponding to the upper plot.

C. Energy spectrum in real space

In order to find the energy spectrum in real space through the BdG transformation, we write the Hamiltonian in the form,

$$\mathcal{H} = \mathbf{C}^\dagger \mathbf{H} \mathbf{C}, \quad (21)$$

where

$$\mathbf{C} = (c_1 \ p_1 \ c_1^\dagger \ p_1^\dagger \ \cdots \ c_N \ p_N \ c_N^\dagger \ p_N^\dagger)^T \quad (22)$$

and the matrix \mathbf{H} is defined as

$$\mathbf{H} = \begin{pmatrix} \mathcal{H}_{11} & \cdots & \mathcal{H}_{1N} \\ \vdots & \ddots & \vdots \\ \mathcal{H}_{N1} & \cdots & \mathcal{H}_{NN} \end{pmatrix}, \quad (23)$$

and is comprised by the following (4×4) interaction matrices

$$\begin{cases} \mathcal{H}_{r,r} & = -\mu\Gamma_{z0}, \\ \mathcal{H}_{r,r+1} & = -t\Gamma_{zz} - i\Delta\Gamma_{yx} + iV\Gamma_{zy}, \\ \mathcal{H}_{r,r-1} & = -t\Gamma_{zz} + i\Delta\Gamma_{yx} - iV\Gamma_{zy}, \\ \mathcal{H}_{r,r'} & = 0 \quad \forall r' \neq r, r+1 \text{ or } r-1. \end{cases} \quad (24)$$

The BdG transformation,

$$\begin{aligned} c_r &= \sum_n [u_{s,n}(r)\gamma_n + v_{s,n}^*(r)\gamma_n^\dagger], \\ p_r &= \sum_n [u_{p,n}(r)\gamma_n + v_{p,n}^*(r)\gamma_n^\dagger], \end{aligned} \quad (25)$$

diagonalizes the Hamiltonian, $\mathcal{H} = E_0 + \sum_n E_n \gamma_n^\dagger \gamma_n$, such that,

$$\mathbf{U}^\dagger \mathbf{H} \mathbf{U} = \mathbf{E}, \quad (26)$$

where \mathbf{U} is formed by all the BdG coefficients u_s , v_s , u_p and v_p , and has the property to be unitary $\mathbf{U}^\dagger \mathbf{U} = \mathbb{I}$. The matrix \mathbf{E} is diagonal and contains the energy spectrum (E_n) of the system.

We have calculated the energy spectrum for a chain of $L = 100$ sites with two-orbitals per site and inter-band interactions in the presence of hybridization. The spectrum consists of $4L$ energies. We have checked that this size is large enough to prevent finite size effects. We set the chemical potential to zero $\mu = 0$, and take the hybridization strong enough ($V > V_c$ or $\Delta = 0$), such that the system is in the TI phase of the phase diagram in Fig. 2b. We can see in Fig. 5a the appearance of zero energy fermionic modes (see below). We also checked that these zero energy modes are localized at the ends of the chain, see Fig. 5b. This gapped insulating phase share the same properties of the topological insulating phase found in a normal sp chain [13–15]. In this situation the fermionic modes resemble the Majorana zero modes, as will be discussed in the next section.

Next, we remove the chemical potential from zero and keep ($V > V_c$), but such that the system remains in the TI phase. We now find that there are two (plus two particle-hole symmetric) energies in the spectrum displaced from zero energy, corresponding also to localized edge states but of finite energy and longer spatial extent.

A more intriguing situation happens when we induce superconductivity on this TI phase and other energies (for a small range of parameters) displaced from the spectrum appear, see figure 5 down left panel. The system now have 4 localized states (plus 4 particle-hole symmetric) consisting of two double-degenerate states. We also show that all those particular energies are localized in the end of the chain, but with lower occupation number each, see down right panel of figure 5.

IV. TOPOLOGICAL INVARIANTS AND EDGE MODES

A. WSC - topological invariant

The winding number is a proper topological invariant that classifies the topological phase of a gapped 1D system. In the gapless superconducting phase, it is not possible to calculate this by conventional methods since

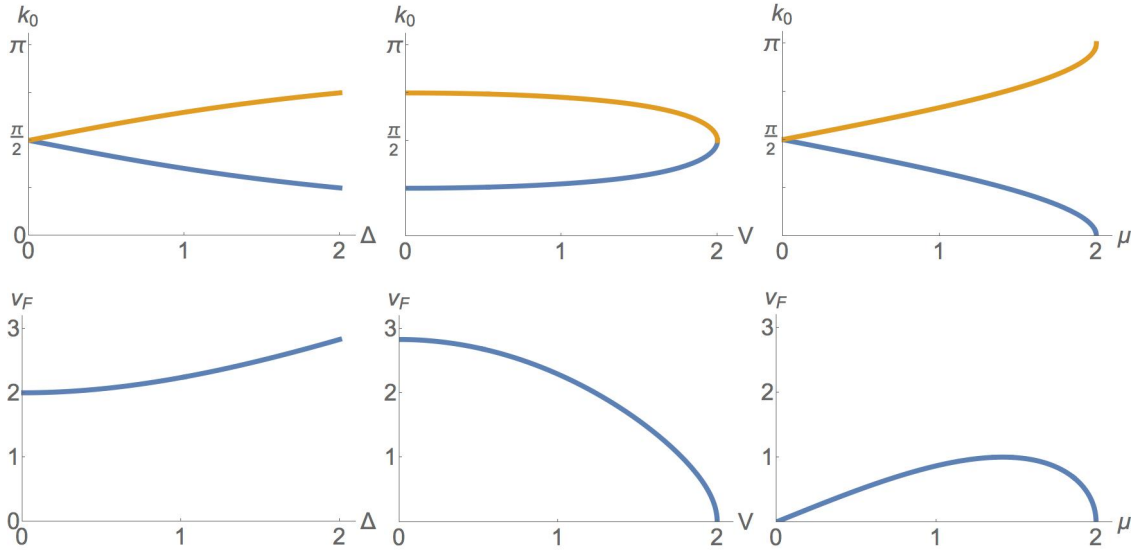


Figure 4. Up row shows the positive Dirac points for a half-filled system ($\mu = 0$) without hybridization ($V = 0$), for a system with fixed superconductivity value ($\Delta = 2$), and for fixed hybridization and superconductivity ($\Delta = V = 2$) when increasing the chemical potential, respectively from left to right. The down row shows the Fermi velocity for each case, corresponding to its upper plot.

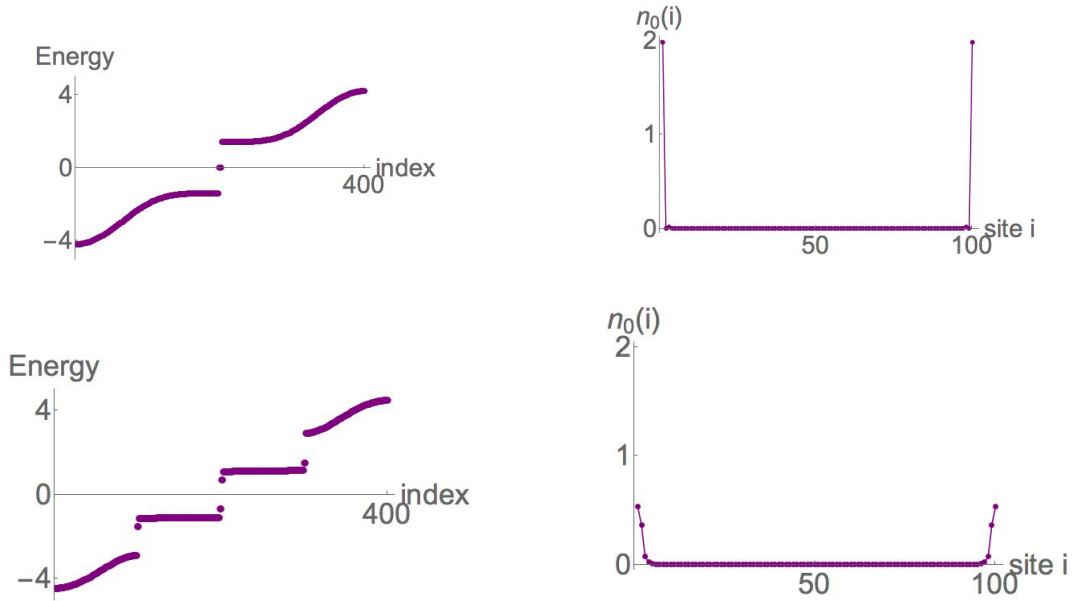


Figure 5. Energy spectrum in real space for a chain of $L = 100$ sites. In the first row, the left panel shows a hybridised system with no, or weak induced, superconductivity when the chemical potential is fine-tuned to zero, $\mu = 0$. The isolated point is four-fold degenerated. On the right, the panel shows the localisation of the Majorana zero modes. In the second row, the left panel shows the same system, with induced superconductivity, but the chemical potential has its value near to zero. Those isolated points are two-fold degenerated. The right panel shows the occupation number on each lattice site for one of those isolated energies. It is clear that they are localised states at the edge.

there are zero energy points that cannot be avoided in one dimensional systems, or the sum over the Brillouin zone gives a vanishing winding number since the Fermi points appear in pairs and their contributions cancel out

[29]. On the other hand, let's look closer to one of the linear dispersion relations (see fig. 3) that crosses the zero energy at some point $k = k_0$. In this region the Hamiltonian with Weyl nodes in 1D can be reduced to

describe the two Bogoliubov bands that cross zero energy. The reduced low energy part of the Hamiltonian may be expanded in terms of Pauli matrix such that

$$H(k) = \sum_{i=1,2,3} d_i(k) \sigma_i. \quad (27)$$

Imposing inversion and charge conjugation operations [29] we end up with only one independent term, for example, $d_z(k) \sim (k - k_0)$, where $\pm k_0$ are the two gapless points and the Hamiltonian is simply

$$H = (k - k_0) \sigma_z = \delta_k \sigma_z. \quad (28)$$

For a positive chemical potential the energy at the Fermi level is positive, which yields the eigenstate of matrix σ_z to be $+1$ or -1 depending on the momentum k , such that $\sigma_z \psi = -\psi$ if $k < k_0$ and $\sigma_z \psi = +\psi$ otherwise. In this frame the winding number can be calculated as [30]

$$W = \text{sgn}(\delta_k) (\psi^{-1} \sigma_z \psi). \quad (29)$$

Therefore, $W = +1$ indicates a non-trivial phase with topological excitations, the Weyl nodes. Note that if the system is not Weyl-like the Hamiltonian cannot be written in terms of one independent component and the winding number value is no longer preserved. Furthermore, the above result is valid not only in the Pauli basis but also for higher order matrices, provided that codimension is zero [29], such as the 4×4 Hamiltonian here considered.

Let us look for a special case of half-filling bands and no hybridization, $\mu = V = 0$. In this situation we are in the WSC phase where the Weyl fermions appear at the momenta $k = \pm\pi/4$ and $k = \pm 3\pi/4$, when $\Delta \approx 2t$. If we make a basis rotation on eq. (3) such that $C_k^\dagger = (c_k^\dagger p_{-k} c_{-k} p_k^\dagger)$ it is easy to see that it can be decoupled in two 2×2 Hamiltonians. Near to the Weyl point k_0 , one of these two Hamiltonians, e.g., the one for the basis $(c_k^\dagger p_{-k})$, is

$$H = (\alpha_0(k - k_0) + m_0) \sigma_0 + (\alpha(k - k_0) + m) \sigma_y, \quad (30)$$

with $\alpha_0 = m_0 = 2t/\sqrt{2}$ and $\alpha = m = \Delta/\sqrt{2}$. Disregarding the mass term m_0 which leads to a shift on the energy, we have only one independent term, the mass term m , which cannot produce a gap by itself on the spectrum.

B. TI - Majorana modes

In order to clarify the existence of Majorana modes in our model, we write the Hamiltonian, Eq. 1, in real space. This is given by,

$$\begin{aligned} \mathcal{H} = \sum_i \left\{ -\mu (c_i^\dagger c_i + p_i^\dagger p_i) + t (p_i^\dagger p_{i+1} - c_i^\dagger c_{i+1}) \right. \\ \left. + V (c_i^\dagger p_{i+1} - c_{i+1}^\dagger p_i) + \Delta (p_i c_{i+1} - p_{i+1} c_i) \right. \\ \left. + \text{h.c.} \right\}. \quad (31) \end{aligned}$$

This can be written in terms of Majorana operators, $\alpha_{A,r}$, $\alpha_{B,r}$, $\beta_{A,r}$ and $\beta_{B,r}$, via the relations,

$$c_r = \frac{1}{2} (\alpha_{B,r} + i\alpha_{A,r}) \quad \text{and} \quad p_r = \frac{1}{2} (\beta_{B,r} + i\beta_{A,r}). \quad (32)$$

Now, we perform a second transformation on Majorana fermions – we call them unconventional hybridized Majorana fermions [31] – such that

$$\alpha_{A,r} = \frac{\gamma_{A,r}^+ + \gamma_{A,r}^-}{2\sqrt{(V - \Delta)}}, \quad \alpha_{B,r} = \frac{\gamma_{B,r}^+ + \gamma_{B,r}^-}{2\sqrt{(V + \Delta)}}, \quad (33)$$

$$\beta_{A,r} = \frac{\gamma_{A,r}^+ - \gamma_{A,r}^-}{2\sqrt{(V + \Delta)}} \quad \text{and} \quad \beta_{B,r} = \frac{\gamma_{B,r}^+ - \gamma_{B,r}^-}{2\sqrt{(V - \Delta)}},$$

the result is the following,

$$\begin{aligned} \mathcal{H}' = \frac{i}{4} \sum_r \left\{ (1 - C_t) (\gamma_{B,r}^- \gamma_{A,r+1}^+ - \gamma_{A,r}^- \gamma_{B,r+1}^+) \right. \\ \left. - (1 + C_t) (\gamma_{B,r}^+ \gamma_{A,r+1}^- - \gamma_{A,r}^+ \gamma_{B,r+1}^-) \right. \\ \left. - C_\mu (\gamma_{B,r}^+ \gamma_{A,r}^+ + \gamma_{B,r}^- \gamma_{A,r}^-) \right\}, \quad (34) \end{aligned}$$

where $C_t \equiv t/\sqrt{(V^2 - \Delta^2)}$ and $C_\mu \equiv \mu/\sqrt{(V^2 - \Delta^2)}$. If we go to the limit $\mu = 0$ and take $C_t = 1$, such that the system is in the TI phase in Fig. 2b ($V > \Delta$), the Hamiltonian reads,

$$\mathcal{H}' = -\frac{i}{2} \sum_{r=1}^{N-1} (\gamma_{B,r}^+ \gamma_{A,r+1}^- - \gamma_{A,r}^+ \gamma_{B,r+1}^-), \quad (35)$$

which couples Majorana fermions only at adjacent lattice sites. Proceeding with the same analysis as [9], we may easily see that the Majorana modes $\gamma_1 = \gamma_{A,1}^+$, $\gamma_2 = \gamma_{B,1}^-$, $\gamma_3 = \gamma_{B,N}^+$, and $\gamma_4 = \gamma_{A,N}^-$ are not present in the above Hamiltonian, it means that they have no cost of energy to be added to the system; they are called Majorana zero modes. In the present case we have two Majorana zero modes on each end, and they can be combined to form one ordinary fermionic operator at each end as

$$f_1 = \frac{1}{2} (\gamma_1 + i\gamma_2) \quad \text{and} \quad f_N = \frac{1}{2} (\gamma_3 + i\gamma_4), \quad (36)$$

or, naively, we may think of two highly non-local fermionic operators such as

$$f = \frac{1}{2} (\gamma_1 + i\gamma_3) \quad \text{and} \quad f' = \frac{1}{2} (\gamma_2 + i\gamma_4). \quad (37)$$

One may note that this result agrees with the conclusion on figure 5 up right panel. Moreover the Majorana zero modes persists out of the fine-tuned $C_t = 1$, or $t^2 = V^2 - \Delta^2$, provided $\mu = 0$, since we know from section II A that there is no gap closing for this range of parameters.

When $\mu \neq 0$, the topological character is preserved, in the sense that we still have localized states at the ends of

the chain, but the Majorana zero modes are not robust such that they acquire a finite energy, see down left panel of figure 5. In this situation, or when general referring, we call them by fermionic modes, instead of Majorana ones.

C. TI - topological invariant

The non-trivial topological character of the TI phase, can be shown by calculating the *winding number* for the special case $\mu = 0$. In this region of the phase diagram we have $\Delta = 0$ and the 4×4 Hamiltonian can be decoupled in two 2×2 Hamiltonians, such as

$$\mathcal{H} = -V_k \sigma_y - \varepsilon_k \sigma_z. \quad (38)$$

This equation can be rewritten as the Hamiltonian of a spin $1/2$ in a k -dependent magnetic field,

$$\mathcal{H} = -\mathbf{h}(k) \cdot \sigma, \quad (39)$$

where $\mathbf{h}(k) = (h_x, h_y, h_z) = (0, -V_k, -\varepsilon_k)$ with the properties $h_{x,y}(k) = -h_{x,y}(-k)$ and $h_z(k) = h_z(-k)$. The winding number ν is obtained as the product of the signs of the *magnetic field* on the center and at the extreme of the Brillouin zone, i.e.,

$$\nu = \text{sgn}(\mathbf{h}(k=0)) \text{sgn}(\mathbf{h}(k=\pi)). \quad (40)$$

Since $\mathbf{h}(k=0) = (0, 0, 2t)$ and $\mathbf{h}(k=\pi) = (0, 0, -2t)$, we get $\nu = -1$, which characterizes the non-trivial topological character of the TI phase along the line $\mu = 0$. The topological nature of this phase is associated with the existence of zero energy modes at the ends of the chain, as discussed above in sec. IV B and also calculated and shown in figure 5.

As μ increases, we observe from the numerical solution that the end modes persist on the chain but acquire a finite energy. As $\mu/2t = 1$, where the gap of the TI phase vanishes, they merge with the continuum of excitations.

If one calculate the winding number (by usual methods) for the whole system, the 4×4 Hamiltonian including Δ , it shows itself trivial. The topology is hidden by the charge conjugation (or particle-hole) symmetry imposed to the system. Some attempts to calculate the winding number using new methods were proposed to uncover this kind of topology. [32]. On the other hand, the topological character of the whole TI phase is guaranteed since it is adiabatically connected with the topological case just shown (when $\Delta = \mu = 0$).

V. CONCLUSIONS

We have studied in this work a 1D *sp*-chain with attractive inter-band interactions and anti-symmetric hy-

bridization due to the different parities of the *s* and *p* orbitals. The latter was shown to be responsible for the appearance of topological phases [14, 15] in non-interacting *sp*-chains. We have shown that this model presents a rich phase diagram including non-trivial topological phases. It is interesting to compare it with the Kitaev model which also has an exact solution. In both models there is a weak coupling superconducting phase with non-trivial topological properties. However, while in Kitaev's model this phase is gapped, in our model it has Fermi points with gapless excitations.

We have studied the quantum topological phase transition between the weak coupling, non-trivial to the trivial, strong coupling superconductor and found that this transition in our model is in a different universality class from that of Kitaev's model. In the strong coupling limit, the superconductivity disappears if μ is very large. We have also shown the existence of a discontinuous quantum phase transition from a Weyl superconductor to a topological insulator with increasing hybridization. This is caused by the appearance of a zero energy mode exactly at the *Fermi surface* of the normal, non-interacting system.

We have shown that in the phase diagram of the present model there is a topological insulating phase, with zero energy fermionic modes at the ends of the chain. This phase has been characterized by calculating its winding number and the zero energy modes have been found both analytically and numerically.

The importance of models with exact solutions in the theory of topological matter has been now widely recognized. Besides throwing light in many exotic properties of these materials, they serve as guides for obtaining new types of excitations which are protected by topology. The present model, which as we have shown exhibits a rich variety of phases and different types of phase transitions, has many new features that allows for a deeper understanding of topological systems.

ACKNOWLEDGMENTS

The authors would like to thank the CNPq and FAPERJ for financial support and B.A. Bernevig and Griffith M.A.S. for useful discussions. PDS acknowledges partial support from FCT through project UID/CTM/04540/2013

- [1] V. Mourik, K. Zuo, S. M. Frolov, S. R. Plissard, E. P. A. M. Bakkers, and L. P. Kouwenhoven, *Science* **336**, 1003 (2012), <http://www.sciencemag.org/content/336/6084/1003.full.pdf>.
- [2] S. Nadj-Perge, I. K. Drozdov, J. Li, H. Chen, S. Jeon, J. Seo, A. H. MacDonald, B. A. Bernevig, and A. Yazdani, *Science* **346**, 602 (2014), <http://www.sciencemag.org/content/346/6209/602.full.pdf>.
- [3] A. D. K. Finck, D. J. Van Harlingen, P. K. Mohseni, K. Jung, and X. Li, *Phys. Rev. Lett.* **110**, 126406 (2013).
- [4] Y. Peng, F. Pientka, L. I. Glazman, and F. von Oppen, *Phys. Rev. Lett.* **114**, 106801 (2015).
- [5] E. Dumitrescu, B. Roberts, S. Tewari, J. D. Sau, and S. Das Sarma, *Phys. Rev. B* **91**, 094505 (2015).
- [6] S. R. Elliott and M. Franz, *Rev. Mod. Phys.* **87**, 137 (2015).
- [7] A. Y. Kitaev, *Physics-Uspekhi* **44**, 131 (2001).
- [8] A. Kitaev, *Annals of Physics* **303**, 2 (2003).
- [9] J. Alicea, *Reports on Progress in Physics* **75**, 076501 (2012).
- [10] B. A. Bernevig, T. L. Hughes, and S.-C. Zhang, *Science* **314**, 1757 (2006), <http://www.sciencemag.org/content/314/5806/1757.full.pdf>.
- [11] X. Li, E. Zhao, and W. Vincent Liu, *Nat Commun* **4**, 1523 (2013).
- [12] M. A. Continentino, F. Deus, I. T. Padilha, and H. Caldas, *Annals of Physics* **348**, 1 (2014).
- [13] M. Dzero, K. Sun, V. Galitski, and P. Coleman, *Phys. Rev. Lett.* **104**, 106408 (2010).
- [14] M. A. Continentino, H. Caldas, D. Nozadze, and N. Trivedi, *Physics Letters A* **378**, 3340 (2014).
- [15] V. Alexandrov and P. Coleman, *Phys. Rev. B* **90**, 115147 (2014).
- [16] H. P. Xia-Ji Liu, Hui Hu, *Chinese Physics B* **24**, 50502 (2015).
- [17] Y. Cao, S.-H. Zou, X.-J. Liu, S. Yi, G.-L. Long, and H. Hu, *Phys. Rev. Lett.* **113**, 115302 (2014).
- [18] S. A. Yang, H. Pan, and F. Zhang, *Phys. Rev. Lett.* **113**, 046401 (2014).
- [19] G. E. Volovik, *The universe in a helium droplet* (Oxford University Press New York, 2009).
- [20] K. Seo, C. Zhang, and S. Tewari, *Phys. Rev. A* **87**, 063618 (2013).
- [21] S. V. Tyablikov, *Methods in the quantum theory of magnetism* (Plenum, 1967).
- [22] E.-N. Foo and L. G. Johnson, *Surface Science* **55**, 189 (1976).
- [23] E.-N. Foo, M. Thorpe, and D. Weaire, *Surface Science* **57**, 323 (1976).
- [24] E.-N. Foo and H.-S. Wong, *Phys. Rev. B* **9**, 1857 (1974).
- [25] M. A. Continentino, G. M. Japiassu, and A. Troper, *Phys. Rev. B* **39**, 9734 (1989).
- [26] M. A. Continentino, *EPL (Europhysics Letters)* **9**, 77 (1989).
- [27] M. A. Continentino, *Quantum scaling in many-body systems* (World Scientific, 2001).
- [28] D. Nozadze and N. Trivedi, *ArXiv e-prints* (2015), [arXiv:1504.00013 \[cond-mat.str-el\]](https://arxiv.org/abs/1504.00013).
- [29] J. Li, H. Chen, I. K. Drozdov, A. Yazdani, B. A. Bernevig, and A. H. MacDonald, *Phys. Rev. B* **90**, 235433 (2014).
- [30] Private discussions with B. Andrei Bernevig.
- [31] We call them unconventional Majorana operators because they are not valid for the same site, in other words, they do not obey the anti-commutation relations when applied to the same site r , e.g., $\{\gamma_{A,r}^+, \gamma_{A,r}^-\} \neq 0$ as it should be.
- [32] R. Wakatsuki, M. Ezawa, Y. Tanaka, and N. Nagaosa, *Phys. Rev. B* **90**, 014505 (2014).

Appendix A: Gap equation with hybridization

In order to demonstrate the result in Eq. (8) we start calculating the gap equation

$$\Delta = -\frac{4g}{L} \sum_k i \sin(k) \langle p_{-k} c_k \rangle, \quad (\text{A1})$$

that we solved using the fluctuation-dissipation theorem

$$\langle p_{-k} c_k \rangle = \frac{i}{2\pi} \int f(\omega) [\langle \langle c_k, p_{-k} \rangle \rangle^r - \langle \langle c_k, p_{-k} \rangle \rangle^a] d\omega, \quad (\text{A2})$$

where $f(\omega)$ is the Fermi distribution. The retarded and advanced Green functions are obtained from the Greenian $\langle \langle \mathbf{G} \rangle \rangle_k = (\mathcal{H}_\omega)^{-1}$, with $\mathcal{H}_\omega \equiv \omega \mathbb{I}_{4 \times 4} - \mathcal{H}_k$, such that

$$\langle \langle \mathbf{G} \rangle \rangle_k = \frac{\mathbf{F}_k(\omega)}{\det(\mathcal{H}_\omega)}. \quad (\text{A3})$$

With the same basis used in equation (3) the Green function $\langle \langle c_k, p_{-k} \rangle \rangle$ is the (4, 1) element of the Greenian matrix, which can be written as

$$\begin{aligned} (\mathbf{F}_k(\omega))_{4,1} &\equiv -i\Delta_k F_k(\omega) \\ &= -i\Delta_k \left[(\omega - \epsilon_k)^2 - \mu^2 - \Delta_k^2 + V_k^2 \right] \end{aligned} \quad (\text{A4})$$

If one put this into the Eq. (A2), proceed with the integral calculation and takes the zero temperature limit, after some calculations, will find that mean value of the operators is

$$\langle p_{-k} c_k \rangle = \frac{-i\Delta_k}{2(\omega_1^2 - \omega_2^2)} \left\{ \frac{F_k(-\omega_2)}{\omega_2} - \frac{F_k(-\omega_1)}{\omega_1} \right\}, \quad (\text{A5})$$

where

$$\omega_1(k) = \sqrt{Z_1 + 2\sqrt{Z_2}} \quad \text{and} \quad \omega_2(k) = \sqrt{Z_1 - 2\sqrt{Z_2}}, \quad (\text{A6})$$

with

$$Z_1 = \epsilon_k^2 + V_k^2 + \Delta_k^2 + \mu^2 \quad (\text{A7})$$

and

$$Z_2 = (\Delta_k^2 + \mu^2) (V_k^2 + \epsilon_k^2). \quad (\text{A8})$$

If we put this result into the gap equation we find that

$$\frac{1}{4g} = -\frac{1}{L} \sum_k \frac{\sin^2(k)}{2(\omega_1^2 - \omega_2^2)} \left\{ \frac{F_k(-\omega_2)}{\omega_2} - \frac{F_k(-\omega_1)}{\omega_1} \right\}. \quad (\text{A9})$$

We can rewrite the right hand side of the equation above as

$$\begin{aligned} & \frac{1}{(\omega_1^2 - \omega_2^2)} \left\{ \frac{F_k(-\omega_2)}{\omega_2} - \frac{F_k(-\omega_1)}{\omega_1} \right\} = \\ & = \frac{1}{(\omega_1 + \omega_2)} \{ \text{sgn}[A(k) - B(k)] - 1 \}, \end{aligned} \quad (\text{A10})$$

where

$$A(k) = (V_k^2 + \epsilon_k^2) \quad \text{and} \quad B(k) = (\Delta_k^2 + \mu^2). \quad (\text{A11})$$

We may write this result in the compact form

$$\frac{1}{(\omega_1^2 - \omega_2^2)} \left\{ \frac{F_k(-\omega_2)}{\omega_2} - \frac{F_k(-\omega_1)}{\omega_1} \right\} = \frac{-2\delta_k}{(\omega_1 + \omega_2)}, \quad (\text{A12})$$

where

$$\delta_k = \begin{cases} 1 & \text{if } B(k) > A(k), \\ 0 & \text{otherwise.} \end{cases} \quad (\text{A13})$$

Such condition shows that the gap equation to this model is

$$\frac{1}{g} = \frac{1}{L} \sum_k \frac{4 \sin^2(k)}{(\omega_1 + \omega_2)} \delta_k. \quad (\text{A14})$$